

RSC Advances



This is an *Accepted Manuscript*, which has been through the Royal Society of Chemistry peer review process and has been accepted for publication.

Accepted Manuscripts are published online shortly after acceptance, before technical editing, formatting and proof reading. Using this free service, authors can make their results available to the community, in citable form, before we publish the edited article. This *Accepted Manuscript* will be replaced by the edited, formatted and paginated article as soon as this is available.

You can find more information about *Accepted Manuscripts* in the [Information for Authors](#).

Please note that technical editing may introduce minor changes to the text and/or graphics, which may alter content. The journal's standard [Terms & Conditions](#) and the [Ethical guidelines](#) still apply. In no event shall the Royal Society of Chemistry be held responsible for any errors or omissions in this *Accepted Manuscript* or any consequences arising from the use of any information it contains.

Synthesis of fluorescent BCN hybrid nanosheets: A highly efficient fluorosensor for rapid, simple, sensitive Ag⁺ detection

Xiaojia Liu, Yurong Gao, Mengxue Zhang, Xiaoyun Zhang, Suiping Wang, Bo Feng*

College of Chemical Engineering, Xiangtan University, Xiangtan 411105, Hunan Province, China

*Corresponding Authors. E-mail: fengbo@xtu.edu.cn, fengbo5460@hotmail.com; Tel.: +86 731 58298259; Fax: +86 731 58298172.

Abstract:

In this work, we develop a simple and low-cost synthetic strategy to prepare BCN hybrid nanosheets. The conversion of graphene oxide (GO) into BCN hybrid nanosheets is accomplished through a reaction with boric acid and melamine at 600 °C, during which boron and nitrogen atoms are incorporated into the graphene atomic sheets. In the absence of metal ions, the BCN exhibits high fluorescence. However, the addition of metal ions causes fluorescence quenching, this property making BCN possible as a fluorosensor to detect metal ions quantitatively. Because of its high selectivity towards Ag⁺, the BCN can be used as a facile sensing platform for label-free sensitive and selective detection of Ag⁺ in aqueous solution. The whole detection process can be completed within 2 min with a detection limit as low as 16 nM.

1. Introduction

Silver and its derivatives are widely used in electrical, pharmaceutical, photographic, and imaging industries.^{1,2} However, silver ions are present in the most toxic form in aquatic environments. When the concentration of Ag(I) ions is sufficiently high, they can exert harmful side effects to the environment.³ Additionally, Ag(I) ions are heavy

metal ions that can cause pollution to water resources.⁴ Therefore, developing a sensitive and selective sensor for the detection of silver in aqueous media is important. Much effort has been exerted to develop fluorescence chemosensors as an alternative method,⁵⁻⁹ which provides new prospects for sensitivity and selectivity, high accuracy, simple instrumental implementation, easy operation, and non-sample destructing or less cell damaging. However, only few successful examples of molecular probes for Ag⁺ detection are available.^{10,11}

Graphene has emerged as an exciting carbon material because of the properties associated with its two-dimensional structure. Since its discovery, graphene has attracted tremendous attention from both academic and commercial communities because of its long-range conjugation that yields extraordinary thermal, mechanical, and electrical properties.¹²⁻¹⁶ Graphene materials that contain heteroatoms such as nitrogen, sulfur, and boron have been actively pursued and considered the most promising candidates to complement graphene in material applications.¹⁷⁻¹⁹ Particularly, the nitrogen (N) atom, which has a comparable atomic size and five valence electrons for bonding with carbon atoms, has been widely used for the preparation of N-doped graphene materials.²⁰⁻²² N-doped carbon material exhibits high fluorescence and can be used as fluorosensor for metal ion detection.^{23,24} Heteroatom doping can drastically alter the electronic characteristics of graphene and result in unusual properties and related applications. The interest in graphene-based luminescent nanomaterials has been increasing because of their unique properties, such as low toxicity, strong and tunable photoluminescence, high stability, high electrical and thermal conductivity, easy preparation, and others.^{25,26}

In this study, an improved annealing route to make BCN hybrid nanosheets was demonstrated. GO was used as the starting template. Boron and nitrogen atoms were

incorporated by co-annealing with boric acid and melamine. The as-prepared BCN hybrid nanosheets were demonstrated as a very effective fluorescent-sensing platform for a label-free, sensitive, and effective Ag^+ detection with a detection limit of as low as 16 nM.

2. Experimental section

2.1 Materials

AgNO_3 , $\text{Co}(\text{NO}_3)_2$, $\text{Cu}(\text{NO}_3)_2$, NaNO_3 , KNO_3 , $\text{Mg}(\text{NO}_3)_2$, $\text{Ca}(\text{NO}_3)_2$, $\text{Ni}(\text{NO}_3)_2$, $\text{Pb}(\text{NO}_3)_2$, $\text{Zn}(\text{NO}_3)_2$, $\text{Fe}(\text{NO}_3)_3$, $\text{Fe}(\text{NO}_3)_2$, $\text{Hg}(\text{NO}_3)_2$, $\text{Cd}(\text{NO}_3)_2$, $\text{Cr}(\text{NO}_3)_2$ and $\text{Al}(\text{NO}_3)_3$ were purchased from Aladin Ltd. (Shanghai, China). All chemicals were used as received without further purification. All solutions employed in the experiment were prepared using deionized Milli-Q water.

2.2 Characterizations

Fourier transform infrared spectroscopy (FTIR) was performed using IR Affinity-1 (Japan). X-ray diffraction (XRD) analysis was carried out on a BRUKER D8-ADVANCE X-ray diffractometer using Cu (40 kV, 40 mA) radiation. Raman spectra were obtained using a laser confocal Raman spectrometer (LABRAM-010) in the range from 400 cm^{-1} to 2000 cm^{-1} . The morphology of the product was investigated by scanning electron microscopy (SEM) (Hitachi S-4800, Japan) at 5.0 kV accelerating voltage. Transmission electron microscopy (TEM) images were obtained with JEM-3010 (JEOL-3010, Japan). X-ray photoelectron spectroscopy (XPS) was carried out using K-Alpha 1063 type with focused monochromatized $\text{Al K}\alpha$ radiation (1486.6 eV). Fluorescent emission spectra were recorded on a RF-5301PC spectrofluorometer (Shimadzu, Japan). Ultraviolet-visible (UV-vis) spectra were recorded with a UV-1800 spectrophotometer.

2.3 Preparation of BCN

GO nanosheets were prepared by a modified Hummers method as reported in the literature.^{27,28} The obtained GO (0.4 g) was thoroughly mixed with a solution of boric acid (2 g) and melamine (2 g) in anhydrous ethanol (100 mL) by ultrasonic dispersion for 1 h. The mixture was dried at 80 °C over night and then heated to 600 °C (10 °C/min), and kept 600 °C for 2 h in N₂ atmosphere. The sample was cooled to room temperature to obtain the BCN powder. Then the product was washed with deionized water and ethanol several times, and filtered through a PTFE membrane. Finally, BCN powder was obtained by vacuum drying at 60 °C for 24 h. In a typical run, 10 mg of BCN powder was added to 100 mL of nanopure water. After ultrasonic dispersion for 2 h, the precipitate was removed by centrifugation, and the clear supernatant extract was prepared for analysis.

2.4 Detection of Ag ions

The detection of Ag ions was performed at room temperature in aqueous solution. Ag aqueous solutions of different concentrations together with other metal ion solutions were freshly prepared before use. To evaluate the sensitivity towards Ag⁺, different concentrations of Ag⁺ were added into aqueous solutions that contain the same amount of BCN, and the mixed solutions were equilibrated for 3 min before spectral measurements. The photoluminescence (PL) spectra were recorded by operating the fluorescence spectrophotometer at 280 nm excitation wavelength.

3. Results and discussion

3.1 Characterization of BCN

The morphologies of the as-prepared BCN were characterized by SEM and TEM. Fig. 1 (a) displays the SEM image of BCN. The SEM image shows that BCN exhibits a layered structure similar to graphene. A typical TEM images of BCN is shown in Fig. 1 (b) and Fig.1 (c). The low-magnification image in Fig. 1 (b) indicates the presence

of BCN layers similar to few-layered graphene. Fig.1 (c) confirms the the formation of few layer nanosheets.

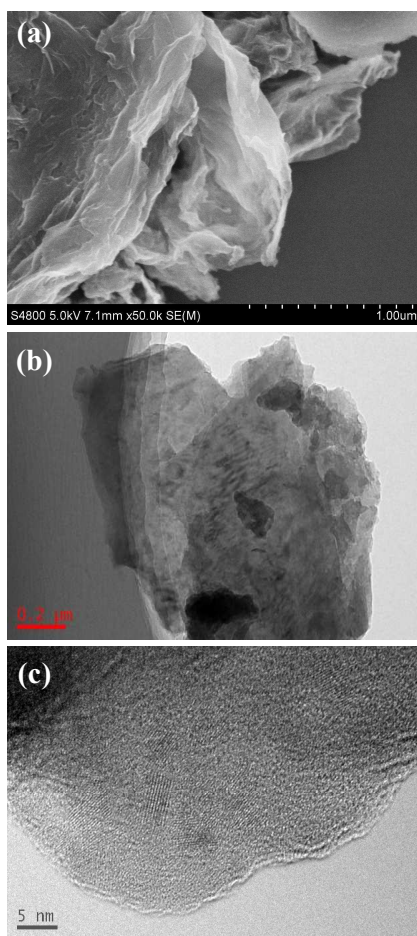


Fig. 1 Typical (a) SEM image of BCN, (b) TEM image of BCN, (c) HRTEM image of the obtained BCN nanosheet.

The compositions of the produced BCN were then characterized by XPS and FTIR. Fig. 2 shows the XPS spectra of BCN. The full spectrum in Fig. 2 (a) indicates the existence of B, C, N, and O elements. The C peak in Fig. 2 (b) can be deconvoluted into five peaks centered at 283.2 (C–B), 284.6 (C–C), 286.2 (C–N), 287.9 (C–O), and 289.2 eV (C–R). The B1s peak in Fig. 2 (c) can be deconvoluted into three peaks at 189.2 (B–C), 191.2 (B–N), and 192.9 eV (B–O). The main peak at 191.2 eV is close to the reported value for B1s (190.75 eV) in BN nanosheets synthesized by CVD

method.²⁹ The N1s peak in Fig. 2 (d) can also be deconvoluted into three peaks corresponding to N–B (397.9 eV), B–N–C (398.6 eV), and graphite–N (401.1 eV).³⁰ Based on the intensity and energy of the major peaks in the B1s and N1s spectra, B and N therefore mainly bond as B–N, which strongly implies the existence of BN domains in the BCN nanosheets. Hence, the chemical formula for BCN is $B_{1.0}C_{6.8}N_{5.3}O_{1.5}$.

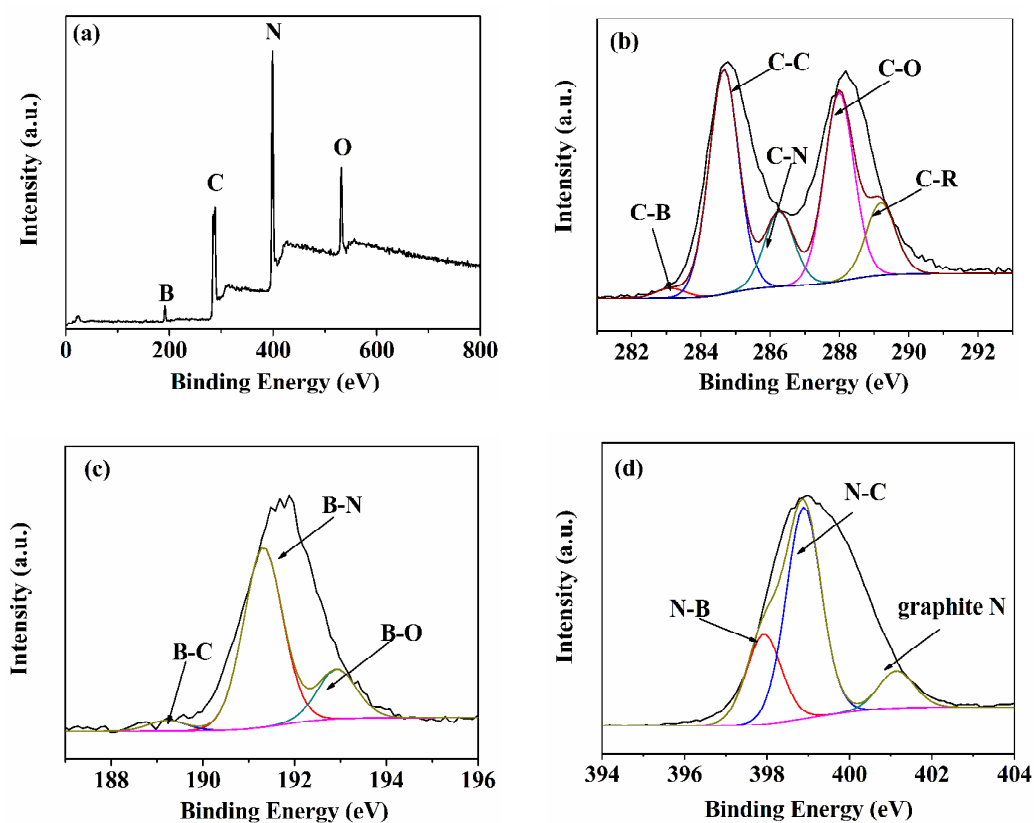


Fig. 2 (a) XPS survey spectra of BCN and XPS spectra of (b) C1s, (c) B1s, and (d) N1s.

The FTIR spectra of GO and BCN are shown in Fig. 3. The GO spectrum shows a strong, broad peak at 3433 cm^{-1} , which indicates the presence of surface O–H stretching vibrations of the C–OH groups and water. The other peaks correspond to C–H groups (2920 cm^{-1}), carboxyl C=O stretching of COOH groups (1720 cm^{-1}), aromatic stretching C=C (1633 cm^{-1}), epoxy C–O group stretching (1213 cm^{-1}),

alkoxy C–OH group stretching vibrations (1052 cm^{-1}), and Ar–H group stretching (834 cm^{-1}). In the BCN spectrum, the as-prepared BCN product exhibits new peaks. The peaks at 1588 and 807 cm^{-1} , at 1385 cm^{-1} , and at 1183 cm^{-1} , correspond to B–N, B–O, and B–C functional groups, respectively. This result indicates that B and N elements functionalize to GO and is highly consistent with the XPS result.

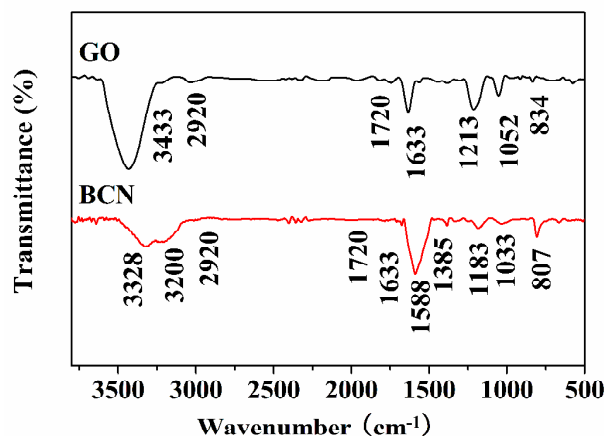


Fig. 3 FTIR spectra of GO and BCN.

Fig. 4 shows the UV–vis absorption and PL emission spectra of the aqueous dispersion of BCN. The UV–vis spectrum shows a strong peak at 204 nm . The dispersion shows a strong PL emission peak centered at 355 nm when excited at 280 nm , thereby indicating that BCN is fluorescent.

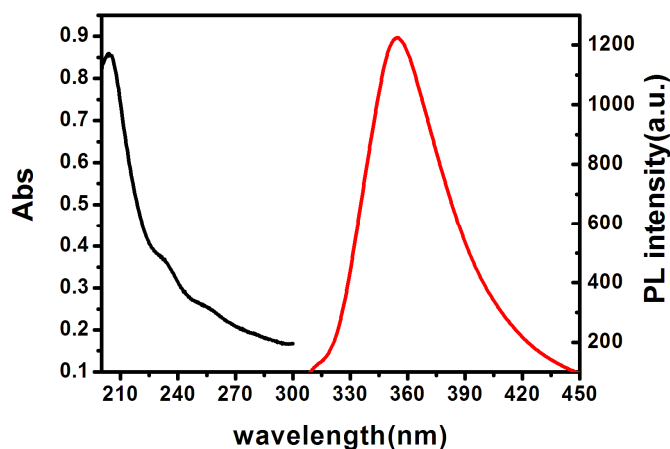


Fig. 4 (a) UV–vis absorption and (b) PL emission spectra of the obtained BCN.

Raman spectroscopy is ideally suited for the characterization of doped graphene.^{31,32} Hence, knowing how it correlates with the concentration of carriers or dopants is important. The shift in the G-band frequency measured by Raman spectroscopy has many physical contributions, and calculations were considered to uncover their relative magnitudes. The Raman spectra show broad D and G bands located at 1345 and 1595 cm^{-1} for GO and at 1345 and 1610 cm^{-1} for BCN, respectively. This result agrees well with some reported literatures about BCN.^{33,34} The I_D/I_G ratio increased from 1.03 for BCN to 1.13 for GO. The increased I_D/I_G ratio for BCN and GO after thermal treatment can be probably attributed to the heteroatom doping that produced new defective sites in the sp^2 carbon frameworks.³⁵

The structural changes of GO and BCN were investigated based on their XRD patterns. Fig. 5 (b) shows the XRD patterns of GO and BCN. After oxidation, a peak at 10.4° is observed, which corresponds to the (001) diffraction peak of GO. According to Bragg's equation ($2d\sin\theta=n\lambda$), the d-spacing of GO increased from 0.3347 nm to 0.8663 nm. This result can be ascribed to the oxide-induced O-containing functional groups that can be confirmed by FTIR. After the reaction with boric acid and melamine, the peak of the product is observed at 26.2° , which corresponds to the (002) diffraction peak of graphite, thereby indicating that BCN has a graphite-like structure.³⁴

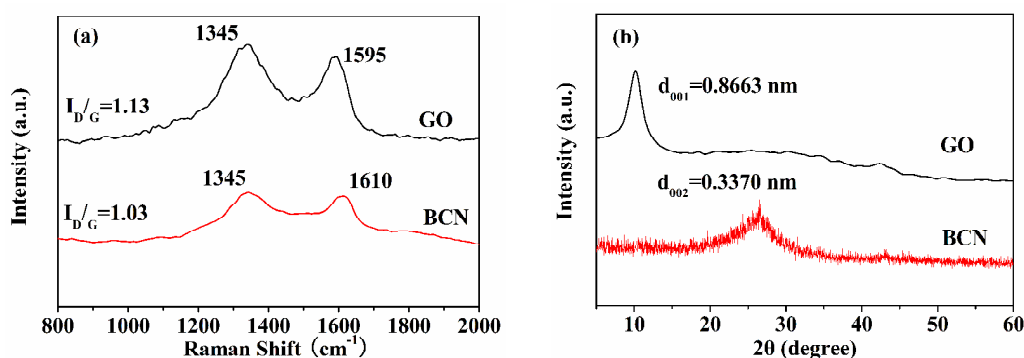


Fig. 5 (a) Raman and (b) XRD spectra of GO and BCN.

3.2 Label-free and highly selective detection of Ag⁺ ions with BCN

The high fluorescence renders BCN a possible promising fluorescence sensor for sensing metal ions. To study the sensitivity of BCN for Ag⁺ detection, the feasibility of using BCN for Ag⁺ detection was explored by adding different concentrations of Ag⁺ to BCN aqueous solution and then measuring the fluorescence intensities. Before using BCN as fluorosensor for detection of Ag⁺, the pH of the detection system were optimized. And the optimization experiment was carried out by monitoring the fluorescence intensity changes of samples in the absence and presence of Ag⁺ (the concentration of Ag⁺ is 6 μ M). The samples were prepared as following: 50 μ L of BCN dispersion was injected into 1950 μ L Tris–HCl buffer to make the final concentration of BCN at 0.15 mg/mL. The result (Fig. S1 in Supporting Information) reveals that BCN is insensitive to pH and the optimum pH is 7–8. Fig. 6 (a) shows the PL spectra of BCN solution with different concentrations of Ag⁺ ions. The result indicates that the PL intensity of the mixture is sensitive to Ag⁺ concentration and decreased with the increase of Ag⁺ concentration. The chelation of Ag⁺ with the N of BCN is believed to bring them into close proximity. Fig. 6 (b) shows the dependence of F_0/F on the concentration of Ag⁺ ions, where F_0 and F represent the fluorescence intensities of BCN at 355 nm in the absence and presence of Ag⁺, respectively. Adding Ag⁺ can lead to an obvious decrease in fluorescence intensity. A good linear correlation was obtained over the concentration range of 0–16 μ M. The detection limit was estimated to be 16 nM at a signal-to-noise ratio of 3.

3.3 Mechanism of fluorescence quenching

To get insight into the fluorescence quenching mechanism involved, the fluorescence quenching data were analyzed by the Stern–Volmer equation:

$$F_0/F = 1 + K_{SV}C.$$

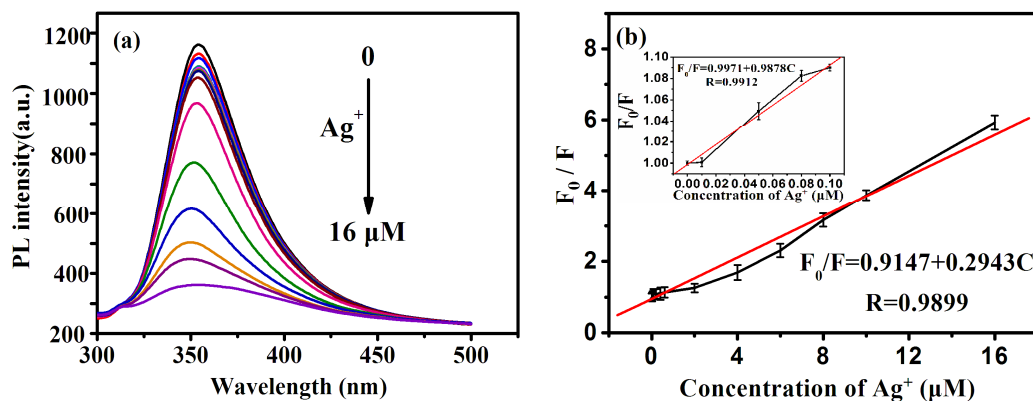


Fig. 6 (a) PL spectra of BCN dispersion with different Ag^+ concentrations (from top to bottom: 0, 0.01, 0.05, 0.08, 0.1, 0.2, 0.4, 0.6, 2, 4, 6, 8, 10, and 16 μM). (b) Stern–Volmer plot for the quenching of BCN by Ag^+ . F_0 and F represent the BCN fluorescence intensities at 355 nm in the absence and presence of Ag^+ ions, respectively.

Where F_0 and F refers to the steady state fluorescence intensities in the absence and in the presence of quencher, respectively. K_{SV} is the Stern–Volmer quenching constant, and C is the quencher concentration. The data are shown in Fig.6 (b) where the ratio F_0/F increases linearly with the Ag^+ concentration and a linear regression equation following Stern–Volmer relation is obtained: $F_0/F = 0.9147 + 0.2943[C]$, with regression coefficient $R = 0.9899$. The linearity of F_0/F versus $[C]$ indicates that only one type of quenching process occurred, either static or dynamic.

To further explore the possible quenching mechanism, the emission lifetime was investigated. Fig. 7 (a) shows the emission lifetime of BCN dispersion in the absence and presence of Ag^+ and there may not be a clear distinction between the two. The analysis of fluorescence decays (Table S1 in Supporting Information) shows that the lifetimes calculated with a two-component decay time model for BCN and BCN-Ag^+ , are not particularly sensitive to the presence of the quencher. The emission lifetime do not depend on the addition of Ag^+ , indicating the static quenching effect over BCN linked to the formation of a stable complex between the fluorophore and Ag^+ .

Furthermore, to distinguish between static and dynamic mechanisms, their differing dependences on temperature have been addressed. One would expect an increase of F_0/F of BCN fluorescence with quencher concentration at higher temperature if collisional quenching predominates. This is because higher temperature results in faster diffusion and hence larger amounts of collisional quenching occurred. Fig. 7 (b) shows the Stern–Volmer plots of BCN fluorescence quenching by Ag^+ at different temperatures. The inset of Fig. 7 (b) shows the relationship between the quenching constant K_{SV} with corresponding temperature. Table S2 in Supporting Information also summarizes the calculated K_{SV} at $T=298, 323$ and 348 K. The results show the Stern–Volmer quenching constant is inversely proportional to temperature, suggesting the probable quenching of BCN– Ag^+ binding reaction is initiated by ground-state compound formation rather than by dynamic collision.³⁶ From above data, we conclude the responsibility of static quenching mechanism as the dominant mechanism of the BCN fluorescence quenching due to the adsorption of Ag^+ to BCN.

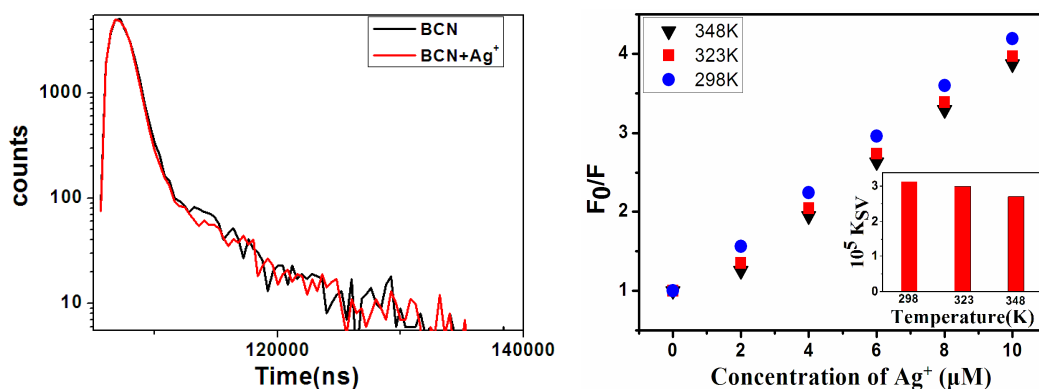


Fig. 7 (a) The emission lifetime of BCN dispersion with the absence and presence of Ag^+ . (b) A Stern–Volmer plot of BCN quenching by Ag^+ at different temperatures, $T=298, 323, 348$ K. The inset shows the relationship between the quenching constant K_{SV} with temperature.

Table 1 compares the sensing performance of different fluorescent probes for Ag^+ ,

showing that our sensing system exhibits superior sensitivity over previously reported sensing systems.

Table 1 Comparison of different fluorescent probes for Ag^+ detection

Fluorescent Probes	Detection Limit (nM)	Linear Range (M)	Ref.
heptamethine cyanine	34	0.6×10^{-7} – 50×10^{-7}	37
CdTe quantum dots	41	4×10^{-7} – 32×10^{-7}	38
DNA and unmodified quantum dots	100	0.2×10^{-8} – 1×10^{-8}	39
tricyanine	200	5×10^{-7} – 2×10^{-5}	40
2,2-disulfediylbis-(N-anthracen-9-ylmethylene) ethanamine (Cysan)	279	0 – 1×10^{-8}	41
coumarin dithioate derivative	400	0.1×10^{-5} – 2.3×10^{-5}	42
BCN	16	0 – 1.6×10^{-5}	This work

The time-dependent plot (Fig. 8) indicates that only 2 min is required to complete the reaction between BCN and Ag^+ . Therefore, the detection is rapid.

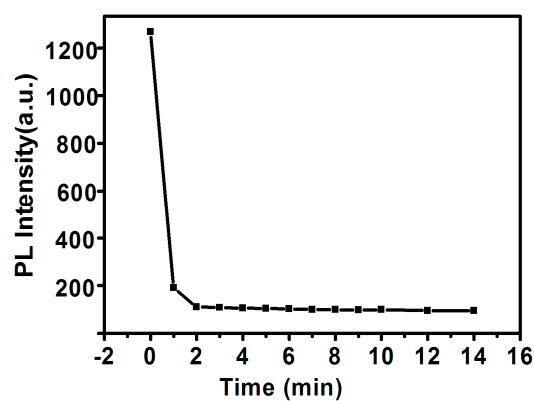


Fig. 8 Fluorescence quenching of BCN by $25 \mu\text{M}$ Ag^+ in solution as a function of time ($\lambda_{\text{ex}} = 280 \text{ nm}$).

Besides sensitivity, selectivity is another important parameter in evaluating the performance of a sensing system. Therefore, to evaluate the selectivity of the sensing

system in this study, the PL intensity changes in the presence of representative metal ions under the same conditions were examined. BCN was added to metal nitrate solutions in pure water and mixed for 10 min to form metal ion–BCN complexes. Fig. 9 shows the PL quenching result of BCN in the presence of Ag^+ , Ca^{2+} , Co^{2+} , K^+ , Zn^{2+} , Cu^{2+} , Ni^{2+} , Pb^{2+} , Mg^{2+} , Na^+ , Fe^{3+} , Fe^{2+} , Hg^{2+} , Cd^{2+} , Cr^{3+} and Al^{3+} . We found that among the tested ions, only Hg^{2+} at a high concentration may interfere with the detection of Ag^+ . Fortunately, this interference can be circumvented by using cysteine (Cys) as masking agent. As shown in Supporting Information Fig. S2, the addition of Hg^{2+} ions into the BCN mixture in the presence of Cys has just slight effect on the detection of Ag^+ . No tremendous decrease was observed with the addition of the metal ions into the BCN solution. However, further addition of Ag^+ into the above mixtures causes a dramatic decrease in PL intensity. All these observations indicate that other metal ions have little impact on the Ag^+ sensing system. The high selectivity of BCN to Ag^+ is due to the fact that Ag^+ has a higher thermodynamic affinity and faster chelating process with the N of BCN than other transition-metal ions.

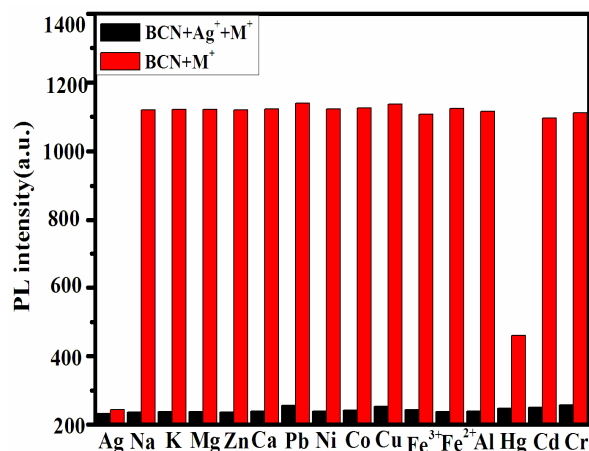


Fig. 9 Selective PL response of BCN after treatment with 25 μM metal ion solutions and interference of 25 μM of other metal ions with 25 μM Ag^+ .

4. Conclusion

We have developed a simple method for the preparation of BCN with boric acid and melamine as boron and nitrogen source, respectively. The synthesized BCN exhibited an enhanced fluorescence. Such BCN has the potential to be used as a novel sensing platform for label-free sensitive and selective detection of Ag⁺ ions in aqueous solutions. However, the fluorescence at 355 nm restricts its scope of biological application.

Acknowledgements

This work is supported by National Natural Science Foundation of China (31270988, 31401577), National Undergraduate Innovational Experimentation Program (201310530007), Scientific Research Fund of Hunan Provincial Education Department (13B120), China Postdoctoral Science Foundation (2014M562118) and Hunan Provincial Natural Science Foundation of China (2015JJ2133, 13JJ9004).

References

- 1 C. Hogstrand and C. M. Wood, *Environ. Toxicol. Chem.*, 1998, **17**, 547-561.
- 2 J. W. Gorsuch and S. J. Klaine, *Environ. Toxicol. Chem.*, 1998, **17**, 537-538.
- 3 H. Li, J. Zhai and X. Sun, *Langmuir*, 2011, **27**, 4305-4308.
- 4 V. K. Bhardwaj, N. Singh, M. S. Hundal and G. Hundal, *Tetrahedron*, 2006, **62**, 7878-7886.
- 5 Y. Wen, F. Xing, S. He, S. Song, L. Wang, Y. Long, D. Li and C. Fan, *Chem. Commun.*, 2010, **46**, 2596-2598.
- 6 C. Liu, S. Huang, H. Yao, S. He, Y. Lu, L. Zhao and X. Zeng, *RSC Adv.*, 2014, **4**, 16109-16114.
- 7 L. Wang, J. Tian, H. Li, Y. Zhang and X. Sun, *Analyst*, 2011, **136**, 891-893.
- 8 C. Cai, H. Cheng, Y. Wang and H. Bao, *RSC Adv.*, 2014, **4**, 59157-59163.

- 9 H. Li, J. Zhai and X. Sun, *Analyst*, 2011, **136**, 2040-2043.
- 10 M. Zhang, B. C. Yin, W. Tan and B. C. Ye, *Biosens. Bioelectron.*, 2011, **26**, 3260-3265.
- 11 C. Zhao, K. Qu, Y. Song, C. Xu, J. Ren and X. Qu, *Chem. Eur. J.*, 2010, **16**, 8147-8154.
- 12 J. Wu, W. Pisula and K. Müllen, *Chem. Rev.*, 2007, **107**, 718-747.
- 13 D. R. Dreyer, S. Park, C. W. Bielawski and R. S. Ruoff, *Chem. Soc. Rev.*, 2010, **39**, 228-240.
- 14 C. N. R. Rao, A. K. Sood, K. S. Subrahmanyam and A. Govindaraj, *Angew. Chem. Int. Ed.*, 2009, **48**, 7752-7777.
- 15 J. Lee, S. Shim, B. Kim and H. S. Shin, *Chem. Eur. J.*, 2011, **17**, 2381-2387.
- 16 M. D. Stoller, S. Park, Y. Zhu, J. An and R. S. Ruoff, *Nano Lett.*, 2008, **8**, 3498-3502.
- 17 O. Stephan, P. M. Ajayan, C. Colliex, P. Redlich, J. M. Lambert, P. Bernier and P. Lefin, *Science*, 1994, **266**, 1683-1685.
- 18 L. Ci, L. Song, C. Jin, D. Jariwala, D. Wu, Y. Li, A. Srivastava, Z. F. Wang, K. Storr, L. Balicas, F. Liu and P. M. Ajayan, *Nat. Mater.*, 2010, **9**, 430-435.
- 19 X. M. Chen, G. H. Wu, Y. Q. Jiang, Y. R. Wang and X. Chen, *Analyst*, 2011, **136**, 4631-4640.
- 20 D. Wei, Y. Liu, Y. Wang, H. Zhang, L. Huang and G. Yu, *Nano Lett.*, 2009, **9**, 1752-1758.
- 21 A. L. M. Reddy, A. Srivastava, S. R. Gowda, H. Gullapalli, M. Dubey and P. M. Ajayan, *ACS Nano*, 2010, **4**, 6337-6342.
- 22 L. Sun, L. Wang, C. Tian, T. Tan, Y. Xie, K. Shi, M. Li and H. Fu, *RSC Adv.*, 2012, **2**, 4498-4506.

- 23 N. Cheng, P. Jiang, Q. Liu, J. Tian, A. M. Asiri and X. Sun, *Analyst*, 2014, **139**, 5065-5068.
- 24 Q. Liu, P. Jiang, Z. Pu, A. M. Asiri, A. O. Al-Youbi and X. Sun, *Sens. Actuators B*, 2014, **194**, 492-497.
- 25 Y. Dong, J. Shao, C. Chen, H. Li, R. Wang, Y. Chi, X. Lin and G. Chen, *Carbon*, 2012, **50**, 4738-4743.
- 26 L. Cao, M. J. Meziani, S. Sahu and Y. Sun, *Acc. Chem. Res.*, 2012, **46**, 171-180.
- 27 C. Y. Su, Y. Xu, W. Zhang, J. Zhao, X. Tang, C. H. Tsai and L. J. Li, *Chem. Mater.*, 2009, **21**, 5674-5680.
- 28 X. Li, H. Wang, J. T. Robinson, H. Sanchez, G. Diankov and H. Dai, *J. Am. Chem. Soc.*, 2009, **131**, 15939-15944.
- 29 Y. Shi, C. Hamsen, X. Jia, K. K. Kim, A. Reina, M. Hofmann, A. L. Hsu, K. Zhang, H. Li, Z. Y. Juang, M. S. Dresselhaus, L. J. Li and J. Kong, *Nano Lett.*, 2010, **10**, 4134-4139.
- 30 Z. S. Wu, A. Winter, L. Chen, Y. Sun, A. Turchanin, X. Feng and K. Müllen, *Adv. Mater.*, 2012, **24**, 5130-5135.
- 31 A. Das, S. Pisana, B. Chakraborty, S. Piscanec, S. K. Saha, U. V. Waghmare, K. S. Novoselov, H. R. Krishnamurthy, A. K. Geim, A. K. Sood and A. C. Ferrari, *Nat. Nanotech.*, 2008, **3**, 210-215.
- 32 T. Ohta, A. Bostwick, T. Seyller, K. Horn and E. Rotenberg, *Science*, 2006, **313**, 951-954.
- 33 N. Kumar, K. Moses, K. Pramoda, S. N. Shirodkar, A. K. Mishra, U. V. Waghmare, A. Sundaresan and C. N. R. Rao, *J. Mater. Chem.*, 2013, **A1**, 5806-5821.
- 34 C. N. R. Rao, H. S. S. R. Matte and U. Maitra, *Angew. Chem. Int. Ed.*, 2013, **52**, 13162-13185.

- 35 Y. Kang, Z. Chu, D. Zhang, G. Li, Z. Jiang, H. Cheng and X. Li, *Carbon*, 2013, **61**, 200-208.
- 36 J. R. Lakowicz, in: *Principles of Fluorescence Spectroscopy*, second ed., Plenum Press, New York, 1999, 331.
- 37 H. Zheng, M. Yan, X. X. Fan, D. Sun, S. Y. Yang, L. J. Yang, J. D. Li, and Y. B. Jiang, *Chem. Commun.*, 2012, **48**, 2243-2245.
- 38 T. T. Gan, Y. J. Zhang, N. J. Zhao, X. Xiao, G. F. Yin, S. H. Yu, H. B. Wang, J. B. Duan, C. Y. Shi and W. Q. Liu, *Spectrochim. Acta A*, 2012, **99**, 62-68.
- 39 W. Sun, J. Yao, T. Yao and S. Shi, *Analyst*, 2013, **138**, 421-424.
- 40 C. Y. Li, X. F. Kong, Y. F. Li, C. X. Zou, D. Liu and W. G. Zhu, *Dyes Pigments*, 2013, **99**, 903-907.
- 41 T. Anand, G. Sivaraman, P. Anandh, D. Chellappa and S. Govindarajan, *Tetrahedron Lett.*, 2014, **55**, 671-675.
- 42 H. A. El-Shekheby, A. H. Mangood, S. M. Hamza, A. S. Al-Kady and el-Z. M. Ebeid, *Luminescence*, 2014, **29**, 158-167.